



New method and tool for increasing fatigue life of a large number of small fastener holes in 2024-T3 Al alloy

J. T. Maximov¹ · G. V. Duncheva¹ · A. P. Anchev¹ · I. M. Amudjev²

Received: 9 October 2018 / Accepted: 26 March 2019 / Published online: 2 April 2019
© The Brazilian Society of Mechanical Sciences and Engineering 2019

Abstract

A new method and tool for processing a large number of small fastener holes in high-strength Al alloy structures through cold plastic deformation have been developed in order to decrease labor and operational time by following the high fatigue resistance requirement. The deforming portion of the tool has been specifically profiled in cross section so that the contact with the hole surface is disrupted. The diameter of the circumference around the deforming portion is greater than the diameter of a preliminary drilled and reamed hole. The tool and hole have a common axis around which the tool is rotating and, at the same time, moving along the same axis while passing through the hole. Thus, this method produces three main beneficial effects: hole cold expansion, surface plastic deformation (mixed burnishing) and microstructure modification (friction stir and torsion). These three effects have been studied and proven through an experiment and 3D FEM simulations. An integral evaluation of the proposed method and tool has been made through fatigue tests of cyclic tension. The obtained S–N curves prove that the fatigue life increases significantly in comparison with the case of only drilled and reamed holes. Based on the conducted studies, a super-combined tool that consequently performs drilling, reaming and cold plastic deformation has been designed and manufactured. This tool significantly increases the productivity of processing a large number of fastener holes in aluminum structures.

Keywords 2024-T3 Al alloy · Fatigue life enhancement · Hole cold expansion · Surface plastic deformation · Cyclic tensile test · FEM simulations

List of symbols

A_5	Elongation	N	Number of cycles to failure
d	Diameter of the circle inscribed in the contour of the cross section of the tool deforming portion	P	Tensile load
d_0	Diameter of the hole after reaming	r	Radius of curvature
D	Diameter of the circle circumscribed over the tool deforming portion	R	Load ratio
E	Young's modulus	R_a	Surface roughness
f	Feed rate	R_z	Height of the initial roughness
h	Height of workpiece	v	Burnishing velocity
i	Interference fit (tightness)	x_i	Governing factors
n	Strain hardening coefficient	Y	Objective function
		z	Number of the tool walls
		ϵ_{\log}	Logarithmic strain
		ϵ_{nom}	Nominal strain
		ν	Poisson's ratio
		σ	Remote stress
		σ_{nom}	Nominal stress
		σ_t	Hoop stress
		σ_{true}	True stress
		σ_u	Ultimate stress
		σ_y	Yield limit

Technical Editor: Márcio Bacci da Silva, Ph.D.

✉ J. T. Maximov
maximov@tugab.bg

¹ Department of Applied Mechanics, Technical University of Gabrovo, 5300 Gabrovo, Bulgaria

² Department of Mechanical Engineering, Technical University of Gabrovo, 5300 Gabrovo, Bulgaria

Abbreviations

CNC	Computer numerical control
FEM	Finite element method
FSHE	Friction stir hole expansion
HCE	Hole cold expansion
MSM	Microstructure modification
SB	Slide burnishing
SPD	Surface plastic deformation

1 Introduction

High-strength aluminum alloys, including 2024-T3, are primarily found in building structures where a high fatigue resistance and high strength to weight ratio are among the main requirements. Airplane structures are one such example as they are characterized by a large number of fastener holes. In order to increase fatigue resistance, these holes are processed through a cold plastic deformation, most often using the split sleeve method [1]. This process is time-consuming, and it requires a skilled technician to accomplish. Since not all fastener holes are loaded at a maximum, this method is only employed where it is absolutely necessary. The other, “less responsible” holes, could be processed using a different method—one that does not reduce the metrics of quality to an unacceptable level (especially the high fatigue resistance metrics), but it drastically decreases all costs related to processing a large number of holes, thus increasing the efficiency of processing. This is why, a new method and tool for cold plastic deformation of fastener holes need to be developed in order to reduce labor and time by keeping the high fatigue resistance standards at the same time.

Based on the “friction stir hole expansion” method (FSHE), a concept for processing a large number of “less responsible” fastener holes has been developed in [2]. The essence of the FSHE method can be summed up as follows: in a preliminary drilled and reamed hole, a conical–cylindrical mandrel is introduced with maximum diameter that is bigger than the diameter of the hole; the mandrel rotates around its axis (it coincides with the axis of the hole), and it moves along that axis at the same time. Factually speaking, FSHE that has been developed for application on fastener holes in aluminum alloys is based on the famous friction stir processing technique [3, 4].

The well-known methods for processing fastener holes through plastic deformation aimed at increasing fatigue life, in general, lead to the following two effects—macro- and microeffects. The macroeffect is characterized by the introduction of beneficial residual compressive hoop stresses whose aim is to lower the rate of formation of fatigue microcracks. The essence of the microeffect is in modifying the microstructure of the material in the superficial layers of the hole. This is expressed in grain refining, homogenization

and pores reduction. As a result from the microeffect, the plasticity and the fatigue strength of the layers with modified microstructure are increased. The methods known as split sleeve, split mandrel [5], symmetric cold expansion [6, 7] (united under the group of mandrel coldworking methods) and the stress wave method [8, 9] produce an impressive macroeffect, while the microeffect is practically absent. FSHE creates both effects, but the benefit of this method is primarily due to the microeffect, as the macroeffect is significantly smaller in comparison with the one created by the mandrel coldworking and stress wave methods. This is why FSHE is a hybrid method. The microeffect in this method is the result of intensive friction forces between the tool and the hole surface moving in an axial direction. Because of this, the beneficial effect manifests itself in the superficial layer. On the other hand, the continuous contact in the cross section of the hole limits the speed of rotation of the tool. This is so because of the negative impact of the generated heat in the formation of residual compressive hoop stresses. Such a rotation speed limitation leads to a lower productivity of the FSHE method. Using a different kind of hybrid method can result in higher levels of productivity which will provide a sufficient microeffect and a significantly greater macroeffect. Such a method can be the combination of surface plastic deformation (SPD) of the hole with a sliding friction contact and of cold hole expansion. This will interrupt the cross-sectional contact between the tool and the hole surface.

The “deep rolling” finishing process developed by Ecoroll primarily aims to increase fatigue strength, respectively, to increase the fatigue life of the processed surface. In order to achieve this goal, deep rolling simultaneously produces three effects: (1) the introduction of beneficial residual compressive hoop stresses with a depth of 0.8 mm; (2) coldwork; (3) burnishing. In its essence, deep rolling belongs to the SPD methods.

When it comes to the process of deep rolling, SPD of small holes (4 ÷ 12 mm) is a problematic endeavor. It is obvious that diamond burnishing [10] is very difficult to carry out for holes with the aforementioned diameters and interval of variation. The ballizing process [11] is applicable to small holes, but it is characterized by low productivity. The spherical mandrelling method [12] eliminates the downside of low productivity, but due to the crossing of the axes of the tool and the hole, the length of the hole that can be processed is limited. “Deep rolling” with a hydrostatic sphere cannot be applied to such holes, since the minimum hole diameter that can be processed with the Ecoroll tools is 19 mm [13]. The roller tools of Ecoroll can process holes with a minimum diameter of 4 mm. However, they are carrying out the “roller burnishing” process, which means they are primarily producing burnishing, while the introduced residual stresses and coldwork are rather symbolic. For the

needs of the aircraft industry, Chris et al. [14] have developed a method and a tool for surface finishing of fastener holes in high-tensile 2024-T3 aluminum alloy. The tool allows reaming a hole to an exact final diameter. At the same time, it is carrying out an SPD of the hole in order to introduce beneficial residual compressive stresses. Unfortunately, there are no known reports concerning the experimental verification of the effectiveness of this tool. There is a tool [2], with a K -profile in cross section that has a small interference fit, and it produces a burnishing effect. The effectiveness of applying this tool has not been widely studied.

The present study presents a method and a tool for processing small fastener holes (4–12 mm) through plastic deformation of preliminary drilled and reamed holes. The kinematics of the method (Fig. 1) is the same as of FSHE: the tool and the hole have a common axis; the tool (the workpiece) is rotating around that axis, and it is simultaneously moving in the direction of that same axis, while the workpiece (the tool) remains static. The tool has a conical–cylindrical working part. The circumference diameter around the cylindrical deforming portion is bigger than the one of the preliminary drilled and reamed holes. The tool deforming portion has been profiled in cross section in a suitable way. Thus, the contact between the tool deforming portion and the hole surface is interrupted in cross section.

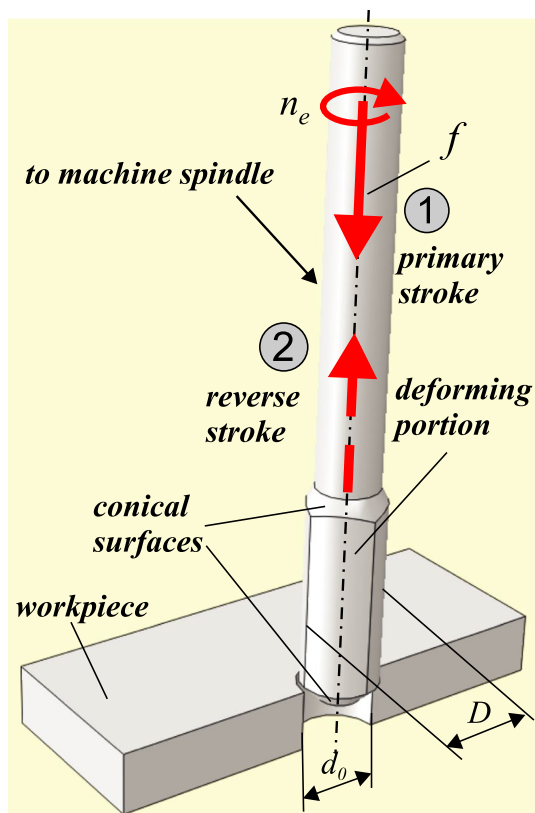


Fig. 1 Kinematics of the proposed method

This method can be utilized using conventional and CNC machine tools, as well as manual machines.

The main purpose of this article is to present the capabilities of the method and tool developed by the authors for increasing the fatigue life of small fastener holes in 2023-T3 Al alloy.

2 Essence of the proposed method and tool

The fastener holes are stress and strain concentrators and, respectively, are potential sites for formation and propagation of fatigue macrocracks. It is known that in flat specimens with holes, subjected to tensile load, the operating stresses in the stress concentrator are approximately three times greater than the nominal ones (Fig. 2). In the presence of dynamic load, the points from the hole surface belonging to the critical cross section are a potential place for formation and propagation of first-mode fatigue macrocracks.

In the process of production of metal workpieces a large number of defects (dislocations) arise in the polycrystals in the microstructure of these metals. Numerous dislocation configurations are formed due to plastic deformations at microlevel with large local microstresses. Due to external cyclical load, these local defects are a cause for nucleation

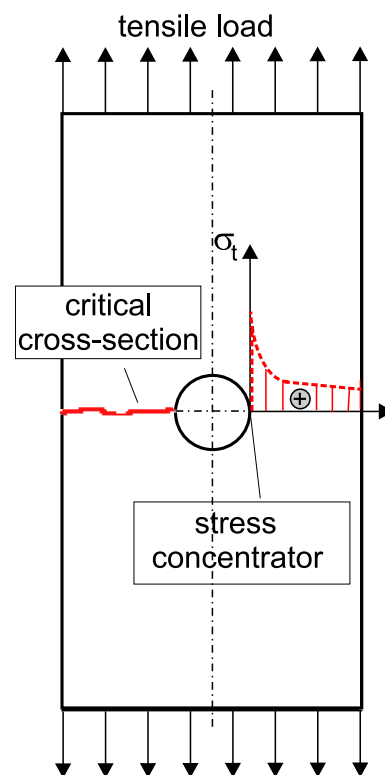


Fig. 2 Stress distribution at critical point of holed structural component undergoing a tensile load

of fatigue microcracks. With prolonged cyclic loading, these microcracks merge and form a fatigue macrocrack with relative magnitude of 100 μm . Under certain conditions the formed macrocrack propagates until the complete destroying of the respective structural or machine element.

At the beginning of the 1920s of the last century, the famous English scientist A. A. Griffith noted that the insufficient strength of the isotropic solids is due to material defects, as the major dimensions of these defects are large compared to intermolecular distances; the effective strength of the technical materials could be increased 10–20 times if these defects could be removed. In the process of producing the metal, and subsequently of the workpiece, eliminating these defects for now is impossible. To obtain a new quality of the material around the fastener holes in order to delay the propagation of the fatigue macrocracks, starting from stress concentrators (see Fig. 2), an impact (mechanical, thermal, chemical or combined) can be applied in the area surrounding the stress concentrator, before the respective components are put into operation. By limiting to mechanical impact, the result of this impact can be expressed in one of the three main beneficial effects (Fig. 3) and combinations thereof:

1. a zone with residual hoop normal stresses around the hole of sufficient depth, that area similarly to a clamp to close the first-mode fatigue macrocrack and thus to delay its propagation;
2. SPD of the hole, producing three beneficial effects simultaneously: introducing residual compressive stresses into the surface and subsurface layers, coldworking and burnishing;
3. modification of the material microstructure around the fastener hole, expressed in grain refining, homogenization and pores reduction.

The three main effects, for the sake of brevity, can be called, respectively, hole cold expansion (HCE); SPD; microstructure modification (MSM).

The HCE effect is created by the so-called mandrel coldworking methods (split sleeve, split mandrel, symmetric cold expansion). Although the essence of the stress wave method is fundamentally different from that of mandrel coldworking methods, stress wave also creates a wide area with beneficial residual stresses around the hole. Mandrel coldworking and stress wave methods increase tens of times the fatigue life of structural components with fastener holes. As a whole, mandrel coldworking methods require special equipment and trained operators. Since these methods require mandatory final reaming, they produce only HCE effect.

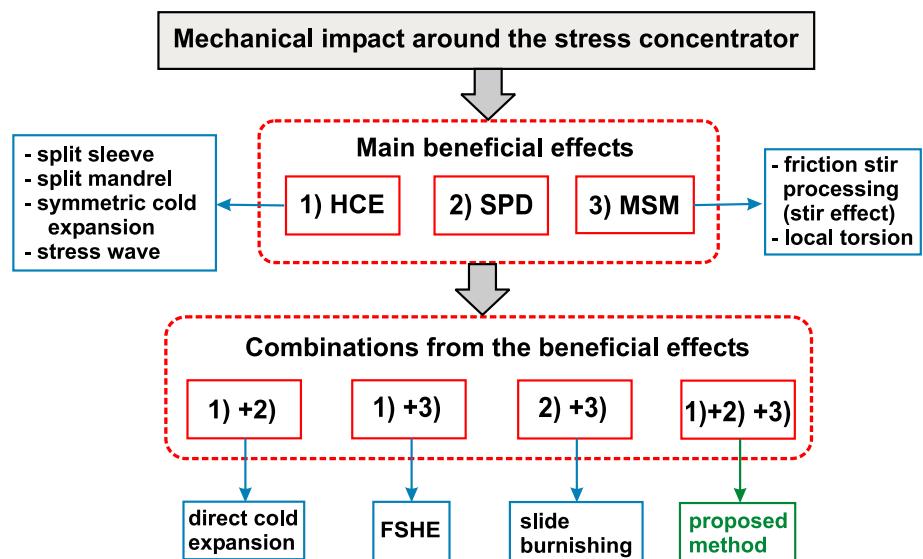
SPD effect is created by the so-called mixed burnishing methods [15, 16]. For instance, it has been proven [17, 18] that slide burnishing (SB) can be applied as mixed burnishing.

MSM effect is created by friction stir processing technique, but this technique in its pure form is not applicable to small holes. Partial friction stir effect of the hole surface is achieved by FSHE method.

Direct cold expansion method (without intermediary between the mandrel and hole surface) produces a combination of HCE and SPD effects. FSHE method produces a combination of CHE and MSM effects. SB of Al alloys is mixed burnishing. In other words, SB combines SPD and MSM effects.

In accordance with the concept of processing a large number of fastener holes [2], the present paper proposes a hybrid method that combines the three major beneficial effects (HCE, SPD and MSM) and requires no special equipment and trained operators. Although the kinematics of the proposed method (see Fig. 1) is the same as that of the FSHE

Fig. 3 Morphological table—justification of the proposed method



method, the new quality is due to the new tool. Figure 4a shows the deforming portion of the new tool. The cross section of the deforming portion has such a profile that allows the contact with the hole surface to be interrupted. The difference between the diameter D of the circle circumscribed over the tool deforming portion (see Fig. 4a) and the hole diameter d_0 , obtained after reaming, provides the necessary interference fit i (tightness), without which the process of cold plastic deformation cannot be carried out. To carry out “cold expansion” of the hole, the interference fit i must be greater than the initial roughness height R_z of the hole surface. At the same time, in order to ensure a discontinuous contact in cross section, the condition $d_0 > d$ needs to be fulfilled, where d is the diameter of the circle inscribed in the contour of the cross section of the tool deforming portion. Therefore, the three diameters and the height R_z of the initial roughness are related to the dependence: $(D - R_z) > d_0 > d$. The edges of the deforming portion have a radius r . The geometry of the tool is designed for unidirectional rotation. SPD is realized by the deforming portion edges of the tool, creating a rotating deformation wave. Each point from the machined hole surface is subjected repeatedly to the impact of deforming edges, which is a prerequisite for significant coldwork of the surface layer. The interrupted contact in cross section is a reason for reaching a lubricant to each point from the hole surface, respectively, is a prerequisite for beneficial burnishing effect. Achieving MSM effect is due to the sliding friction contact between the tool deforming portion and the hole surface.

In the following sections, using experiment and FEM simulations, the following positive effects, produced by the proposed new method and tool, are evaluated: (1) HCE effect—finding of residual hoop compressive stress distribution around the hole; (2) burnishing effect—finding of the

hole surface roughness depending on the process parameters; (3) coldwork—finding of equivalent plastic strain distribution; (4) MSM effect—evaluation of grain refining and homogenization of the material microstructure immediately around the hole. Finally, an integral evaluation of the effectiveness of the proposed method and tool has been performed through fatigue tests.

3 Experiment

3.1 Evaluation of the burnishing effect

In this section the optimal manufacturing parameters of the process and the number of walls of the tool deforming portion are established under “minimum roughness” criterion. In other words, burnishing effect, produced by the method and tool, has been experimentally studied.

As the fastener holes most often have a diameter within the range $4 \div 12$ mm, the investigations have been made for the middle of the interval, i.e., the nominal diameter of the holes being machined is 8 mm. In order to find the optimal values of the parameters of the cold plastic deformation process, deforming tools are manufactured (Fig. 4b) with different number of walls, respectively, 3, 4 and 5. The geometrical parameters of the deforming portions of the tools are $D = 8.25$ mm, $r = 1$ mm and for the corresponding number of walls $d = 7.8$ mm, $d = 7.88$ mm, $d = 7.94$ mm. The samples are cylindrical with diameter $\varphi 32$ mm and height of 8 mm and are made of 2024-T3 Al alloy with yield limit $\sigma_y = 395$ MPa, ultimate stress $\sigma_u = 551$ MPa and elongation $A_5 = 11.7\%$. The mechanical characteristics are obtained through one-dimensional tensile test. The experiment was carried out on a vertical machine center Haas MiniMill. The

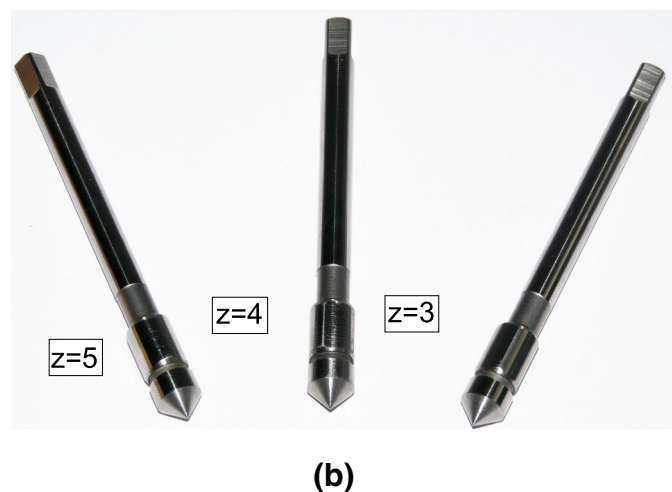
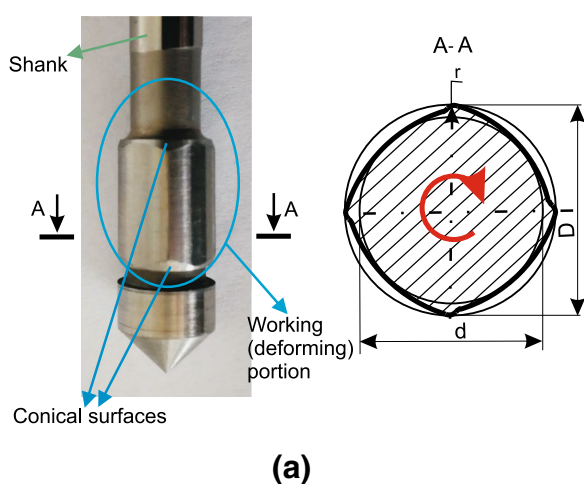


Fig. 4 Deforming tools: **a** tool deforming portion; **b** general view

governing factors of the process are: speed v (the speed of a point from the circle circumscribed over the tool deforming portion); feed rate f ; interference fit (tightness) i (the difference between the diameter D of the circumscribed circle and the hole diameter d_0 , obtained after reaming); number of the walls z of the tool deforming portion. The study was carried out in two stages. In the first stage, the factor space was scanned in order to determine the rational ranges of variance of the governing factors and to determine the optimum initial roughness (after drilling and next reaming). Based on this, the second stage was devoted to a planned experiment. The objective function was the roughness obtained R_a . The latter is measured by surface roughness tester SRT—6210.

The initial hole drilling was carried out by a drill of 7.8 mm diameter. The hole obtained diameter was 7.95 mm. Then, the hole was reamed with feed rate 0.3 mm/rev and frequency of rotation 400 rpm/min, which ensures average value of the roughness obtained $R_a = 1.4 \mu\text{m}$. In order to establish the rational ranges of variation of the governing factors, scanning the factor space was performed using a one-factor-at-a-time method. Interference fit $i = 0.05 \text{ mm}$ was used. It was assumed that the influence on the roughness of each of the other factors does not depend on the interference fit. Based on the first-stage experimental results, the following conclusions were made:

- As the feed rate increases, the roughness obtained increases monotonically (Fig. 5a). This result confirms the observed tendency for the influence of the feed rate on the roughness in all finishing processes. With increasing the speed, the roughness shows a tendency to a slight decrease (Fig. 5b);
- It is noteworthy that the odd number of sides of the deformation tool leads to higher surface roughness (Fig. 5c). From the point of view of the roughness obtained, it is expedient to use a tool with a number of walls equal to four;
- Of the three factors, the influence of the speed on the roughness obtained is the most insignificant.

The preliminary experiment gave enough information to define the levels of factor variation in the actual part of the experimental study, namely the planned experiment. The latter was conducted using three governing factors: feed rate f , speed v and number of walls z . The objective function was roughness obtained R_a . The interference fit was $i = 0.05 \text{ mm}$. The levels of variation of the governing factors are shown in Table 1. The preliminary experiment showed that the roughness depends nonlinearly on each factor. For this reason an optimal composed second-order design was chosen (Table 2). Three attempts were made for each experimental point. The resulting roughness values are shown in Table 2.

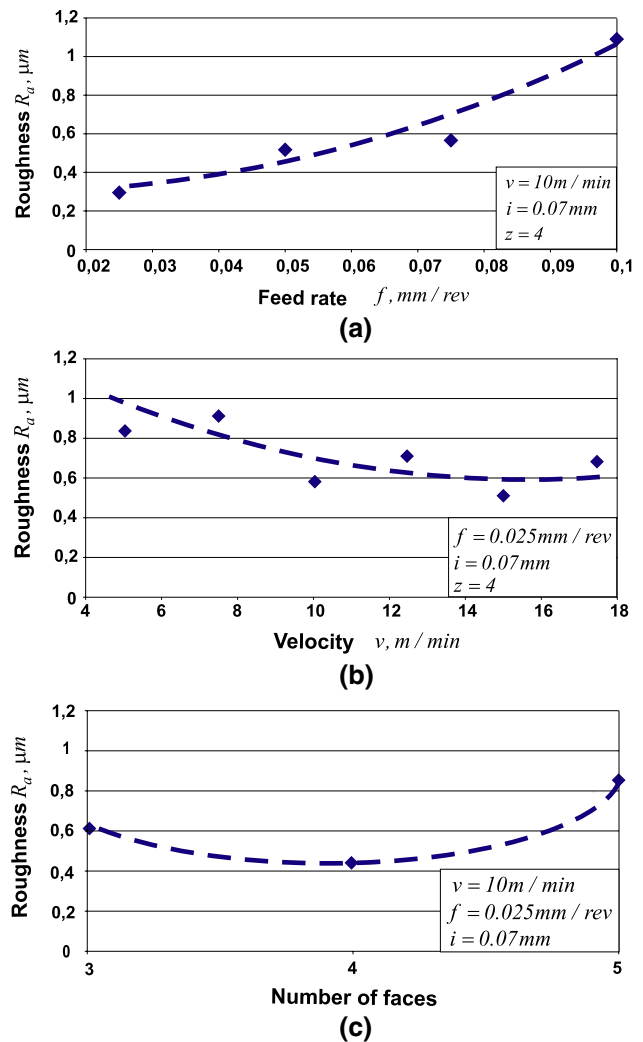


Fig. 5 Roughness obtained from one-factor-at-the-time experiment

Table 1 Governing factors and levels

Governing factors	Factor levels			
	Coded			
		-1	0	+1
Natural	Coded	Natural		
Feed rate $f, \text{mm/ob}$	x_1	0.025	0.05	0.075
Velocity $v, \text{m/min}$	x_2	7.5	15	22.5
Number of walls z	x_3	3	4	5

Analysis of variance (ANOVA) was conducted in order to study the factor influence (Fig. 6), using QStatLab. The outcomes are shown in Table 3. The most significant factors (see Fig. 6a) are x_1 and x_3 (feed rate and number of walls), and most insignificant factor is x_2 (speed). Obviously, with increasing the feed, the resulting roughness increases. When

Table 2 Experimental design

No.	x_1	x_2	x_3	R_a^{init} , μm	$\{R_{a,u}\}_1$	$\{R_{a,u}\}_2$	$\{R_{a,u}\}_3$	$\{R_{a,u}\}_{\text{aver}}$
1	-1	-1	-1	1.4	0.622	0.709	0.484	0.605
2	1	-1	-1		0.753	0.925	1.030	0.902
3	-1	1	-1		0.936	0.654	0.601	0.730
4	1	1	-1		0.709	2.04	1.68	1.476
5	-1	-1	1		0.549	0.676	0.434	0.553
6	1	-1	1		0.695	0.679	0.613	0.662
7	-1	1	1		0.741	0.354	0.518	0.537
8	1	1	1		0.805	0.799	0.796	0.8
9	-1	0	0		0.353	0.478	0.422	0.417
10	1	0	0		0.701	0.924	0.563	0.729
11	0	-1	0		0.4	0.690	0.489	0.526
12	0	1	0		0.646	0.343	0.790	0.593
13	0	0	-1		1.320	1.465	1.454	1.413
14	0	0	1		0.491	0.93	0.959	0.793
15	0	0	0		0.392	0.487	0.528	0.469

the number of walls is $z = 3$, the roughness is maximum. The roughness decreases sharply when the number of walls is $z = 4$. Obviously the interaction between the factors x_1 and x_3 (feed rate and number of walls) is the most significant (see Fig. 6b).

Regression analysis was performed using QStatLab. Given the type of the experimental design, the regression model was chosen to be a second-order polynomial. The following regression model was obtained:

$$\begin{aligned}
 Y_{R_a} = & 0.65015 + 0.1727x_1 + 0.0888x_2 \\
 & - 0.1781x_3 - 0.12394x_1^2 - 0.13744x_2^2 + \\
 & + 0.40606x_3^2 + 0.07537x_1x_2 \\
 & - 0.07212x_2x_3 - 0.08387x_1x_3
 \end{aligned} \quad (1)$$

The dependence between coded x_ℓ and natural \tilde{x}_ℓ factors is:

$$x_\ell = (\tilde{x}_\ell - \tilde{x}_{0,\ell}) / \lambda_\ell \quad (2)$$

where $\lambda_\ell = (\tilde{x}_{\text{max},\ell} - \tilde{x}_{\text{min},\ell}) / 2$, $\tilde{x}_{0,\ell}$, $\tilde{x}_{\text{max},\ell}$ and $\tilde{x}_{\text{min},\ell}$ are, respectively, average, upper and lower levels of ℓ th natural factor. After substituting (2) in (1), the expression of roughness in natural form is obtained. The analysis of the regression model is performed using sections of the hypersurface (1) with different hyperplanes (Fig. 7). Obviously, the deforming tool with number of walls $z = 3$ is not appropriate due to the high roughness that is produced. When $z = 3$ the contact area between the deforming tool and the hole surface is the smallest. As a result, the deformation wave in the circumferential direction has a relatively large height. This results in a reduction in the useful burnishing effect. A lower surface roughness is obtained when $z = 4$ compared to the case when $z = 5$. The further increase in the number of walls leads to degraded lubricant conditions,

which results in deterioration of the roughness obtained. On this basis the optimal values of governing factors are chosen as follows: $f = 0.025$ mm/rev, $v = 22.5$ m/min, $z = 4$. Using these values of the governing factors, the effect of the interference fit on the roughness obtained was studied. Four groups of samples (each containing 10 samples) were treated, respectively, with $i = 0.05$ mm, $i = 0.07$ mm, $i = 0.09$ mm and $i = 0.11$ mm. The obtained mean value of the measured roughness of the respective groups was, respectively, $R_a = 0.511$ μm , $R_a = 0.476$ μm , $R_a = 0.694$ μm and $R_a = 0.105$ μm . Obviously, the quality of the treated surface is sharply deteriorated, when $i > 0.09$ mm. Therefore, the interference fit is limited to $i = 0.09$ mm in the subsequent studies.

3.2 Evaluation of the MSM effect

The microstructure evolution is depicted in Fig. 8. The first specimen (Fig. 8a) was subjected to drilling and reaming. The average grain size near the surface layer is approximately 20 μm . After drilling and reaming, the hole of the second specimen was processed through the new method and tool, using interference fit $i = 0.07$ mm and optimal values of the governing factors (Fig. 8b). The microstructure at a depth of about 0.3 mm is highly deformed. The field near the hole surface, subjected to greater plastic deformation, has changed their texture. Elongation of the grains in hoop direction, parallel to the burnishing velocity, is observed. As a result of the burnishing, a more homogeneous microstructure is observed. The average grain size in radial direction is approximately 7 μm . The microstructure obtained is almost three times refined, compared to the first specimen. At the same time, a greater degree of the microstructure homogenization is noticed in the surface

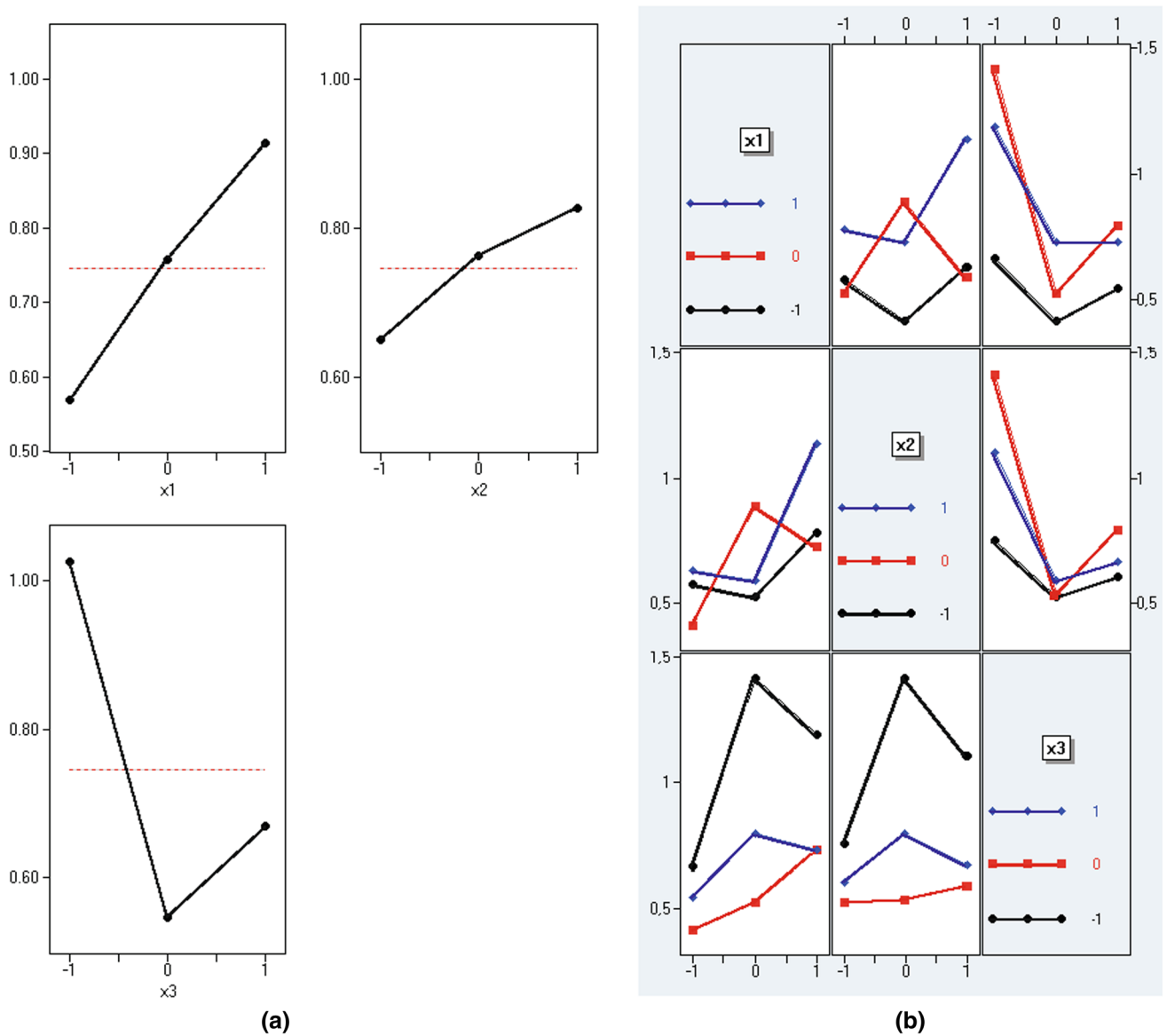


Fig. 6 Outcomes from ANOVA: **a** main effects; **b** interactions between the governing factors

layer. It can be concluded that the optical analysis carried out confirms that slide burnishing of the hole surface refines the grains, homogenizes and reduces pores in the material.

4 FEM simulations

4.1 Formulation of the study

The proposed hybrid method combines the advantages of cold expansion with those of slide burnishing and, respectively, produces all three beneficial effects: HCE, SPD and MSM. It is practically impossible to directly evaluate the latter effect (grain refining, microstructure homogenization

and reduction of the pores in the superficial layer) by means of FEM simulations, since the FEM requires defined geometry and physics of the modeled object, respectively, the integration area. Therefore, only the first two effects (HCE and SPD) can be evaluated through FEM simulations in an aspect of distribution of the introduced residual hoop stresses and the equivalent plastic strain in a depth from the hole surface layer. It should be noted that in the surface layer the residual stresses and the equivalent plastic strain are due to both the cold expansion and the burnishing effect with the sliding friction contact. FEM model, taking into account simultaneously both the cold extension and the burnishing effects in the surface layer defining the initial roughness, creates a very large computational task requiring a lot of

Table 3 ANOVA outcomesAnalysis of variance (ANOVA) for average roughness obtained $R_{a,aver}—(x1; x2; x3)$

Symbol	Name	Number of levels	Levels		
x1	x1	3	−1	0	1
x2	x2	3	−1	0	1
x3	x3	3	−1	0	1
Source	Amounts	Degree of freedom	Dispersion	F	P
x1	0.29916	2	0.14958	3.18629	0.09599
x2	0.08087	2	0.04044	0.86134	0.45837
x3	0.62020	2	0.31010	6.60564	0.02023
Остатък	0.37556	8	0.04694		
Общо	1.37556	14			

Residual mean square deviation (RMSD)=0.21667 R-sq=0.72702 R-sq (adj)=0.52229

Confidence intervals for the average value at each factor level:

(Confidence intervals are based on the standard deviation for each factor level)

Factor	Level	Number	Mean	Dispersion	95% Confidence interval
x1	−1	5	0.56840	0.01290	$0.4274 \leq 0.5684 \leq 0.7094$
	0	5	0.75760	0.14958	$0.2774 \leq 0.7576 \leq 1.2378$
	1	5	0.91380	0.10668	$0.5083 \leq 0.9138 \leq 1.3193$
x2	−1	5	0.64960	0.02261	$0.4629 \leq 0.6496 \leq 0.8363$
	0	5	0.76300	0.15857	$0.2686 \leq 0.7630 \leq 1.2574$
	1	5	0.82720	0.14255	$0.3584 \leq 0.8272 \leq 1.2960$
x3	−1	5	1.02520	0.15812	$0.5315 \leq 1.0252 \leq 1.5189$
	0	5	0.54560	0.01491	$0.3940 \leq 0.5456 \leq 0.6972$
	1	5	0.66900	0.01587	$0.5126 \leq 0.6690 \leq 0.8254$

machine time and operational memory. Therefore, the current FEM study of the proposed hybrid process is carried out in two stages by means of two separate 3D FEM models. The first model contains the complete geometry (without modeling the initial roughness) and the kinematics of the tool–workpiece system and aims to find the distribution of the introduced residual hoop stresses in several cross sections of the workpiece: entrance face, exit face, middle plane and the section containing residual stress with a maximum absolute value. This FEM model also provides information about the power-force parameters of the process, such as torque. The second FEM model provides information about both the formation of residual stresses and the equivalent plastic strain in the surface and subsurface layers, taking into account the influence of the initial kinematic roughness. The equivalent plastic strain in the surface layer is in direct correlation with the resulting microhardness: the larger the strain is, the larger the microhardness is. In other words, the equivalent plastic strain is a measure of the performed coldwork. Therefore, the first FEM model evaluates the HCE beneficial effect, while the second FEM model evaluates the SPD effect. It is important to note that the constitutive models of the workpiece material in the two FEM models

are different, since the surface layer behavior is usually different from that of the bulk material.

4.2 FEM simulation of the whole process

4.2.1 FEM model

a. Common feature

3D FEM model (Fig. 9a) was created to simulate the processing of fastener hole $\varphi 8$ mm through deforming tool with number of walls $z = 4$, using ABAQUS v.6.12.1. The rounded edges of the tool have a radius $r = 1$ mm. Rotational workpiece with height $h = 5$ mm and diameter of the pre-drilled hole $d_0 = 8$ mm was chosen. The workpiece outer surface was selected to be rotational in order to eliminate the boundary effect on the results obtained. The material is 2024-T3 Al alloy. The tool is modeled as rigid body. Only the edges of the tool are modeled as four rotating bodies. The cylindrical portion of each body has a diameter 2 mm. Eight-nodal linear hexahedral FEs of type C3D8R are chosen for the workpiece. The model consists of 4160 FEs and 5040 nodes. FEM simulation is carried out in one basic step. The workpiece is stationary in the

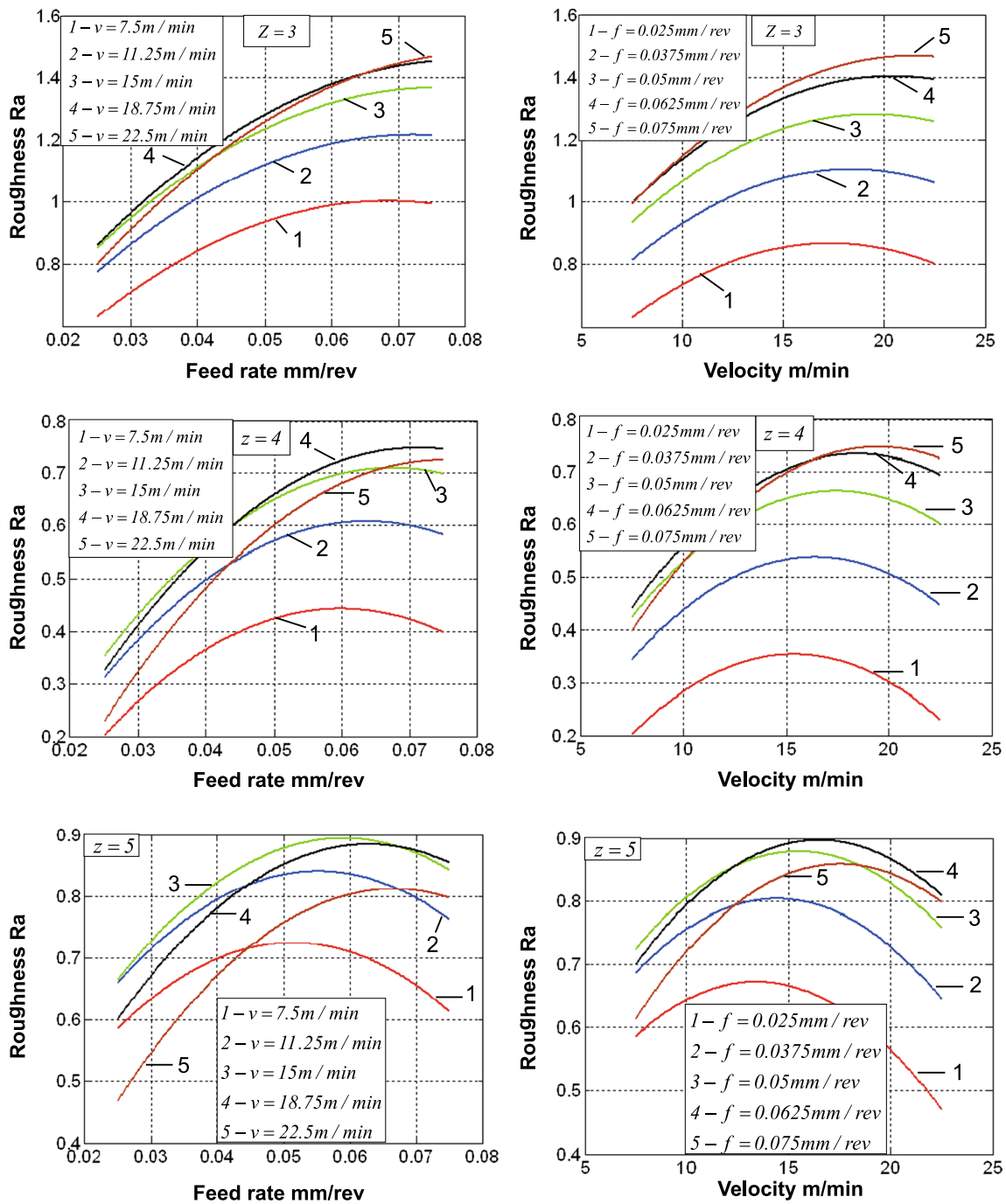


Fig. 7 Sections of the hypersurface of the roughness obtained model with different hyperplanes

global coordinate system. The four bodies rotate synchronously as one rigid body around the workpiece axis and at the same time perform a rectilinear translation along the same axis. The rotation and translation are matched in the pseudo-time to implement the required tool feed rate. The analysis was carried out sequentially with three values of the interference fit: 0.05 mm, 0.07 mm and 0.09 mm.

b. Material constitutive model of the workpiece

Elastic-plastic behavior is assigned of the workpiece, which is made of 2024-T3 Al alloy. The elastic behavior is set by Young’s modulus $E = 0.72 \times 10^{11}$ Pa and Poisson’s ratio $\nu = 0.33$. In the plastic field the material behavior is set as “true stress–logarithmic strain” ($\sigma_{true} - \epsilon_{log}$)

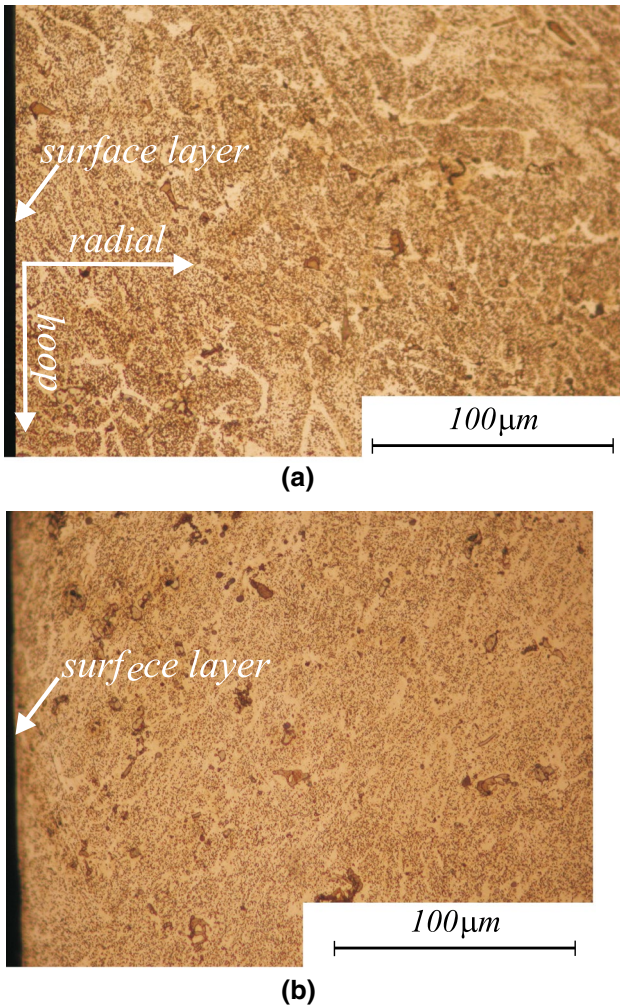


Fig. 8 Optical micrographs near hole surface: **a** only drilled and reamed; **b** treated by new method

tabulated function. For this purpose, by using a one-dimensional tensile test, the “nominal stress–nominal strain” ($\sigma_{nom} - \epsilon_{nom}$) diagram is obtained (Fig. 10). The required tabulated function $\sigma_{true} - \epsilon_{ln}$ is obtained through the equations $\sigma_{true} = \sigma_{nom} (1 + \epsilon_{nom})$ and $\epsilon_{log} = \ln (1 + \epsilon_{nom})$. In fact, it is assumed that the true stress in the plastic field is valid for all stressed states and load paths. Nonlinear kinematic strain hardening of the workpiece material is defined, assuming that the material behavior is independent of the strain velocity.

c. Interactions

Normal contact allowing separation and tangential contact with friction coefficient of 0.08 is defined between the operating tool portion and the workpiece. Constraint of type “coupling” is assigned to the four working bodies. The constraint is expressed in defining a new reference point (RP-1), to which appropriate boundary conditions are assigned.

d. Boundary conditions

Zero displacements along the axes x and z and zero rotations around the same axes are defined for RP-1 (see Fig. 9a). At the same point (RP-1), the displacement along the hole axis (y) and rotation around the same axis is defined by tabulated functions. The pseudo-time is 0.1. The displacement at the pseudo-time end equals 12 mm, and the rotation is equal to 160 rpm. Thus, these displacement and rotation values provide a feed rate of 0.075 mm/rev. The workpiece is stationary fixed, and on the outer cylindrical surface zero displacements are defined in a local cylindrical coordinate system.

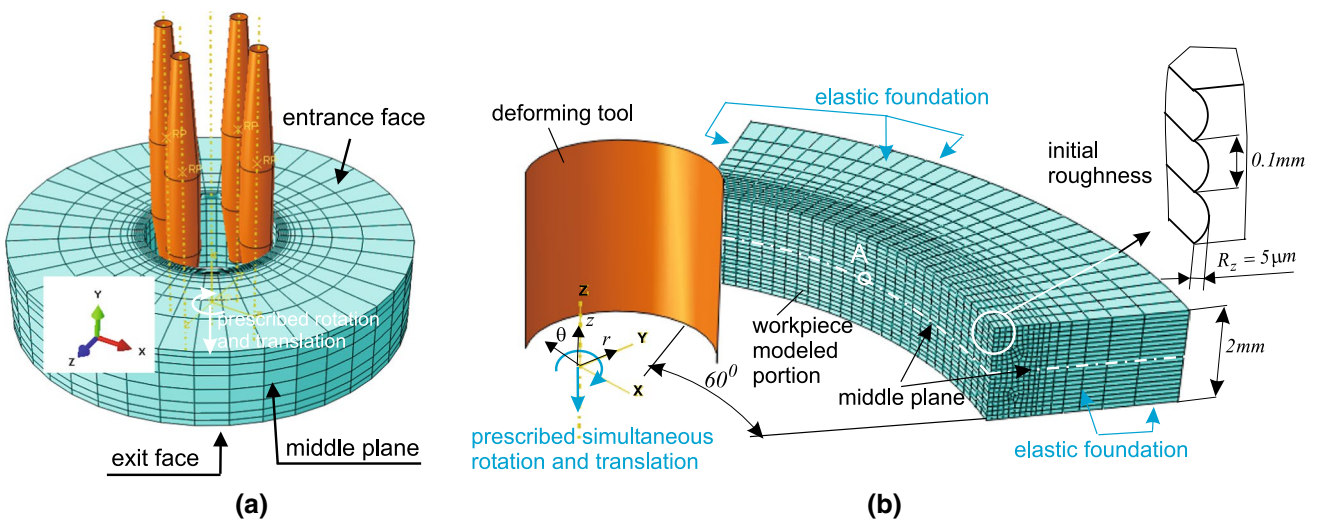


Fig. 9 3D FEM models: **a** of the whole process; **b** of the burnishing portion

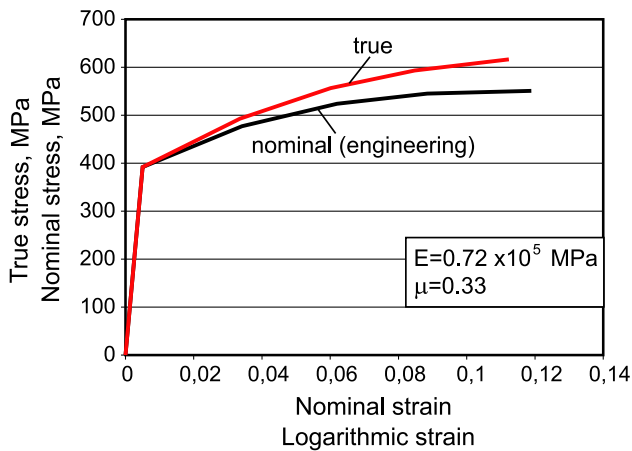


Fig. 10 Stress–strain diagrams of the 2024-T3 Al alloy

4.2.2 FEM results

The residual hoop normal stress distribution in radial direction from the hole edge is shown in Fig. 11, respectively, on the entrance face, middle plane, exit face and plane containing the residual stress with maximum absolute value. For all interference fit values, the following is observed:

- The residual stresses are the smallest in absolute value on the entrance face;
- On the exit face the residual stresses are larger in absolute value as compared to these on the entrance face and the formed compressive area is significantly wider;
- In the middle plane, the residual stresses are very similar in size and distribution to those in the cross section containing residual stress with maximum absolute value. This section lies between the middle plane and exit face;
- The above features are characteristic of mandrel cold-working methods in which a conical–cylindrical mandrel having a larger diameter than that of the hole passes all the way through the hole, creating a significant gradient of residual stresses along the hole axis. The only exception is symmetric cold expansion method, which creates a symmetric compressive zone relative to the middle plane with a minimum axis gradient.
- The smallest interference fit ($i = 0.05$ mm) is obviously insufficient, as a tensile ring is formed around the hole edge on the entrance face. This is a very undesirable effect, as it is a prerequisite for creating corner fatigue macrocrack.
- With increasing interference fit, the residual stresses increase in absolute values and the width of the compressive field also increases. At the same time, the axial gradient of the residual stress distribution also increases, which is an undesirable effect.

It should be noted that the extent to which interference fit can be increased, in addition to the axial gradient of residual stresses, also depends on other factors, such as the power-force process parameters, the equivalent plastic strain in a point from the hole surface, the hole surface roughness and other.

Figure 12 shows the distribution of the rotating moment, applied to the tool shank to implement the process. As expected, with increasing interference fit the maximum torque increases.

4.3 FEM simulation of the burnishing

4.3.1 FEM model

3D FEM model (Fig. 9b) was developed to simulate the burnishing portion of the whole process. Starting from the hole surface, a small part from the workpiece is modeled. The middle plane of the workpiece is a symmetry plane of the modeled portion. The role of the initial roughness (before burnishing) in the FEM model is very important for the resulting characteristics (after burnishing) in the surface layer. The distribution of the peak-to-valley height of the initial surface geometry has a stochastic character. Therefore, in the FEM model the initial kinematic roughness of the hole surface is presented as $R_z = 5$ μm with a step of 0.1 mm. Only one deforming edge from the tool is modeled as rigid body. The FEM model contains 10,020 eight-nodal linear hexahedral FEs of type C3D8R and 120 six-nodal linear wedge FEs of type C3D6. The total number of nodes is 11,439.

The material constitutive model of the superficial layer of 2024-T3 Al alloy is defined in [18] through indentation test and inverse FEM analysis. In the plastic field, the dependence “true stress–logarithmic strain” is defined as follows:

$$\sigma_{\text{true}} = \sigma_{\text{yield}} \left(1 + \frac{E}{\sigma_{\text{yield}}} \varepsilon_{\log} \right)^n$$

where σ_{true} is the true stress, $\sigma_{\text{yield}} = 280$ MPa is the yield limit, $E = 72$ GPa is Young’s modulus, ε_{\log} is the logarithmic strain in the plastic field, and $n = 0.075$ is the strain hardening for a one-dimensional stressed state.

Normal contact allowing separation and tangential contact with friction coefficient of 0.08 is defined between the deforming tool and the hole surface. All surfaces of the modeled portion without the hole surface are placed on an elastic foundation having a coefficient 0.7×10^5 MPa. Thus, the effect of the removed portion from the workpiece on the modeled portion is taken into account. All degrees of freedom of the deforming tool are removed, except for rotation around the axis of the machined hole and displacement along the same axis.

Fig. 11 Residual hoop stress distribution

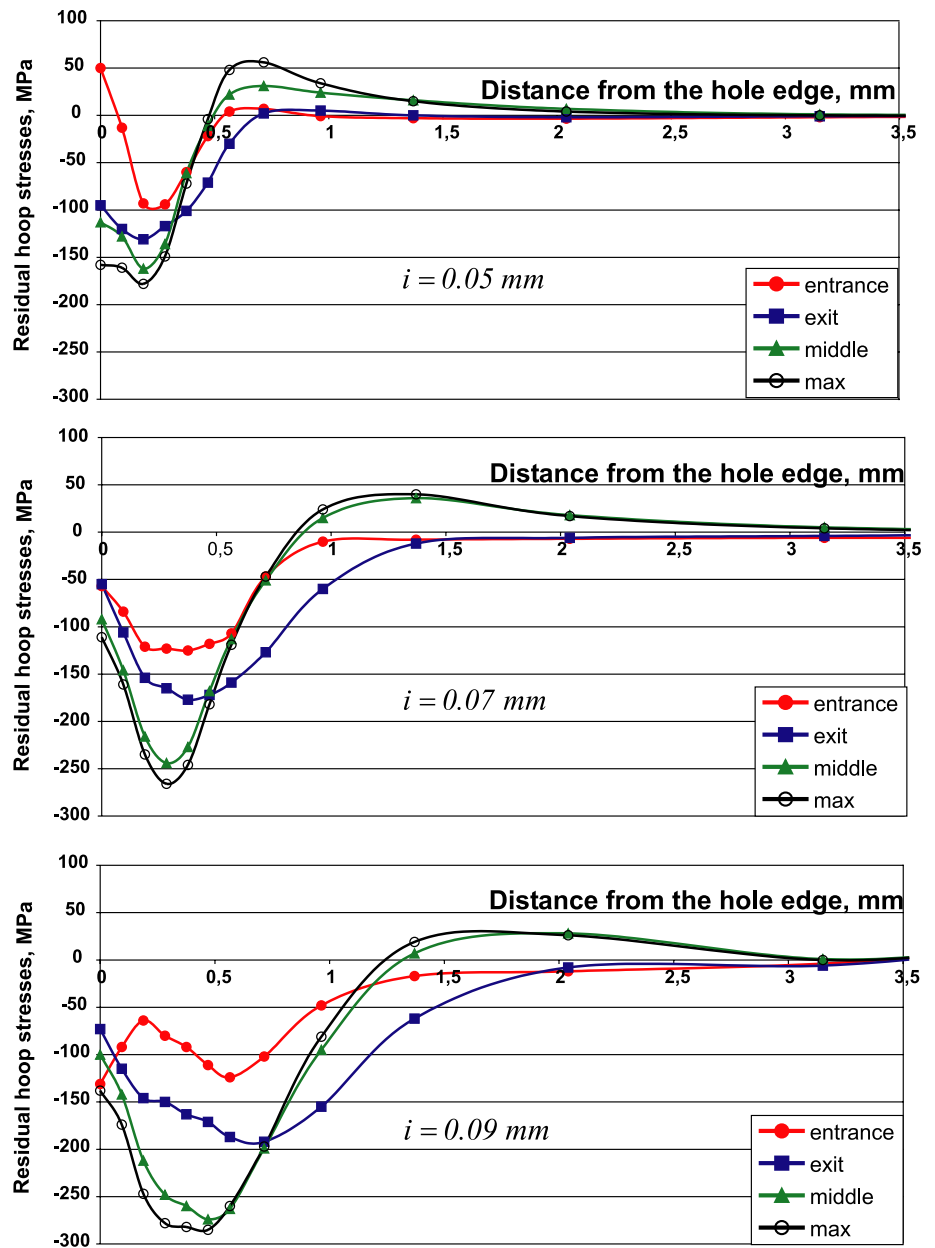
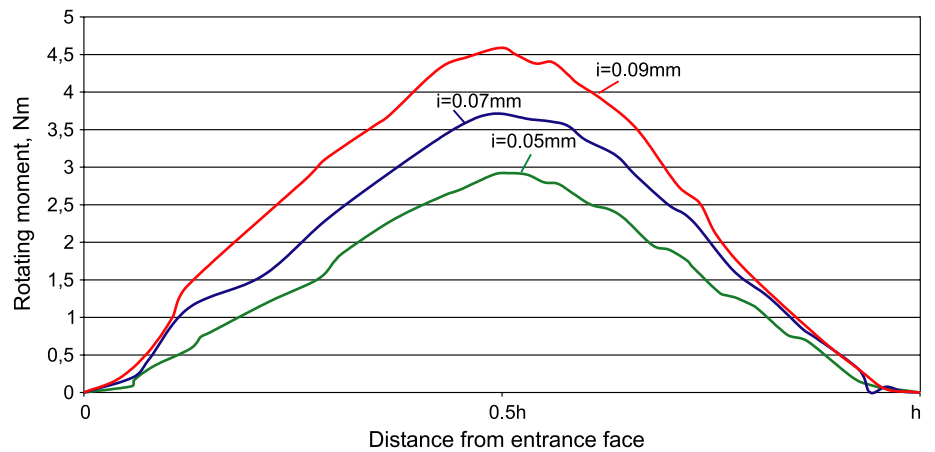


Fig. 12 Variation of the rotating moment



4.3.2 FEM outcomes

Figure 13a shows the equivalent plastic strain distribution in the middle plane in a depth from the hole edge, starting from point A (see Fig. 9b). The distribution has one and the same character for all interference fit values. The maximum value of the equivalent plastic strain is at a depth $0.05 \div 0.08$ mm. On the hole surface the strain is slightly smaller than the maximum value. Once its maximum value has been reached, the deformation rapidly decreases. As expected, with increasing interference fit the maximum strain increases. The conducted strain analysis shows that in a cylindrical coordinate system $r\theta z$ (see Fig. 9b) the components ε_{rr} , $\varepsilon_{\theta\theta}$ and $\varepsilon_{r\theta}$ of the plastic strain in point A are two orders of magnitude larger than the components ε_{zz} , $\varepsilon_{\theta z}$ and ε_{rz} . Therefore, the texture formation of the material microstructure immediately around the hole is carried out in planes parallel to a plane $r\theta$, i.e., perpendicular to the workpiece axis.

The large equivalent plastic strain in the surface and sub-surface layers is a measure of significant coldwork, respectively, of significantly increasing microhardness and grain refining, and is ultimately a condition for increasing the crack resistance of the hole surface. On the other hand, the interference fit cannot grow indefinitely, as the equivalent plastic strain cannot grow indefinitely. It is clear that a further increase in interference fit will lead to local surface ruptures, which is absolutely undesirable as these local defects are potential places for formation and propagation of fatigue macrocracks.

Figure 13b shows the residual hoop displacement distribution in a depth from the hole edge, starting from point A (see Fig. 9b). The maximum values of these displacements are in point A. Therefore, SPD is accompanied by so-called local torsion effect, which causes surface strengthening through grain refining. With other words, the local torsion leads to hole surface modification. Shamdani and Khoddam have been studied idealized cold expansion followed by local torsion process by means of FEM simulations [19]. They simulate the two processes sequentially by definition in all nodes of the hole surface of uniform, respectively, radial and hoop, displacement. The authors prove that the introduction through cold expansion residual hoop compressive stresses undergoes a reduction due to local torsion since this process introduces residual hoop tensile stresses immediately around the hole surface. In the present study, the interaction of the deforming tool and workpiece is simulated by defining the exact kinematics of the method (see Fig. 9a). Therefore, in the present study the carried out FEM simulations of the whole process (simultaneously HCE and SPD with local torsion) provide information on the residual stresses introduced not only by cold expansion. The obtained residual stresses (see Fig. 11) are a consequence of the concurrent

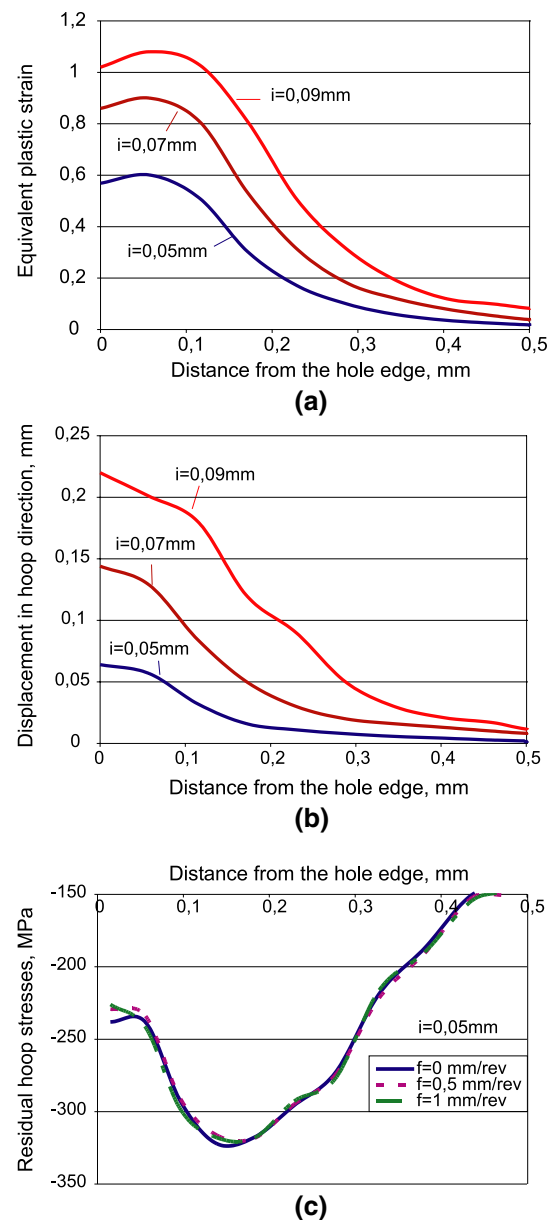


Fig. 13 Distribution in the middle plane: **a** equivalent plastic strain; **b** displacement in hoop direction; **c** residual hoop stresses

action of HCE and SPD with local torsion. In this study, the simulation of burnishing with sliding friction contact, which leads to the creation of local torsion effect, has been done by defining a interdependent rotation and translation of the deforming tool in order to obtain the desired feed rate. It is established that SPD creates a plastic wave, which rotates together with the tool and encompasses successively each point from the modeled portion of the hole surface. As a result, the processed surface turns out to be “twisted,” but the residual hoop stresses are compressive (Fig. 13c) immediately surrounding the hole surface. The impact of the feed

rate on the residual hoop stress distribution obviously has no practical significance. Since the results are very similar, the residual stress values are shown at the points of integration of the respective finite elements in order to eliminate node averaging errors. Compared to Fig. 11 ($i = 0.05$ mm), the obtained residual stresses have a greater absolute value due to significantly more refined FEM mesh.

5 Fatigue tests

5.1 Essence of the study

The purpose of the study is to make an integral assessment of the proposed method and tool effectiveness in terms of increasing the fatigue life of structural components with fastener holes made of 2024-T3 Al alloy. Four groups of specimens, having central hole, were manufactured. The holes of the specimens from the first group, called basic, were processed only by cutting—sequentially drilling and reaming. The holes of the samples from the other three groups were previously drilled and reamed, after which they were processed using the new method and tool under conditions of different interference fit between individual groups. The interference fit was as follows: for the second group—0.05 mm, for the third group—0.07 mm and for the fourth group—0.09 mm. Openings from all groups after treatment had the same nominal diameter of 8.2 mm. All specimens were subjected to a cyclic tensile test to failure, after which an S–N curve was constructed for each specimen group. The effectiveness of the new method and tool was evaluated based on a comparison of the S–N curves obtained.

5.2 Experiment details

5.2.1 Specimens

The specimens were made of 2024-T3 Al alloy and were cut from a sheet so that their longitudinal axes were aligned in the sheet rolling direction. The specimen dimensions are shown in Fig. 14.

5.2.2 Processing of sample holes

The processing was performed on Haas MiniMill vertical machine center. The specimen holes from all groups were drilled with one and the same drill, having a diameter $\varphi 7.9$ mm. The nominal diameters of the reamers for the four specimen groups are as follows: basic group— $\varphi 8.2$ mm; second group— $\varphi 8.2$ mm; third group— $\varphi 8.18$ mm; fourth group— $\varphi 8.16$ mm. The diameter of the circle circumscribed over the tool deforming portion is $D = 8.25$ mm.

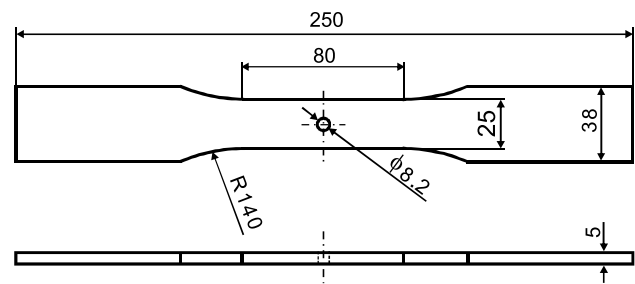


Fig. 14 Fatigue specimen sizes

5.2.3 Fatigue test

The fatigue test was conducted on Instron 1332 testing machine using pulsating cycles, i.e., sinusoidal loads with a load ratio of $R = P_{\min}/P_{\max} = 0$, at a load frequency of 10 Hz. The maximum tensile load P_{\max} creates remote stress σ in the middle part of the specimens away from the hole. The maximum load (peak load) was increased from 9.5 to 14.5 kN, and this resulted in remote stress (peak stress) from 76 to 116 MPa. The samples from each group were subjected to remote stress of, respectively, 116, 108, 100, 92, 84 and 76 MPa up to achieving a failure. For producing a given S–N curve, one sample was tested at each stress amplitude. The minimum number of tested specimens per group was 6. In a case of large scattering of the result obtained for a given experimental point, the experiment with the same amplitude was repeated with extra sample.

In order to find the dependence between the remote stress and the equivalent stress in the critical point from the hole periphery, FEM simulation of the tensile test was carried out. Because of the symmetry, an eighth part (Fig. 15) was modeled from the portion of the specimen with sizes $60 \times 25 \times 5$ mm (see Fig. 14). The dependence obtained is shown in Table 4.

5.3 Results and discussion

The fatigue test results are represented on S–N diagram shown in Fig. 16. On the basis of the obtained fatigue curves the following comments can be made.

- As it was expected, all samples with coldworked holes show a longer fatigue life in comparison with the specimens from the basic group.
- Increasing the interference fit does not lead to a substantial increase in the fatigue life. The probable reason is the introduction of manufacturing defects in the hole surface due to significant plastic strain. Therefore, the increase in the interference fit over $i = 0.07$ mm is meaningless.

Fig. 15 3D FEM model of the tensile test

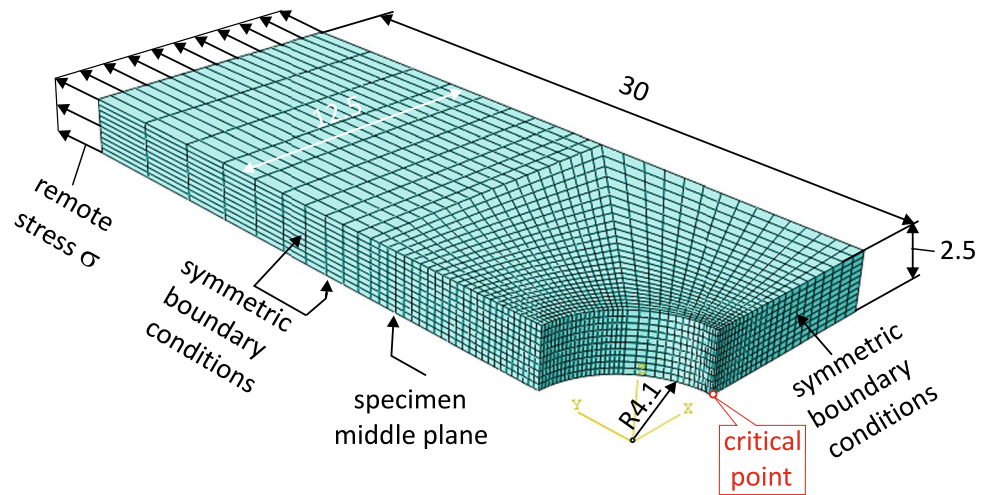


Table 4 Dependence between remote stress and equivalent stress in the critical point

Maximum tensile load, N	Remote stress, MPa	Equivalent stress in the critical point, MPa
14,500	116	385.108
13,500	108	358.61
12,500	100	332.104
11,500	92	305.588
10,500	84	279.063
9500	76	252.525

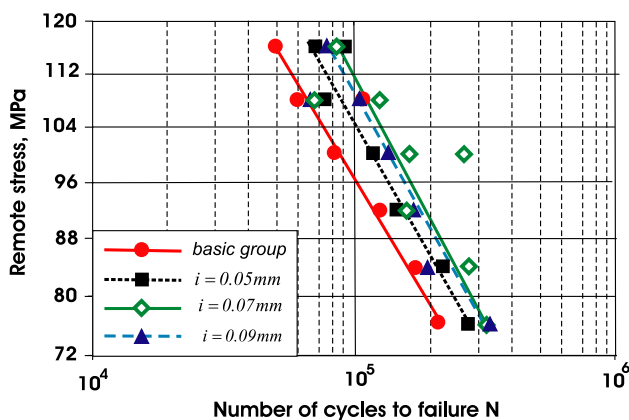


Fig. 16 S–N curves—effect of the interference fit on fatigue life

- The results obtained for the specimens fatigue life prove the benefit of the proposed method and tool.

6 Super-combined tool

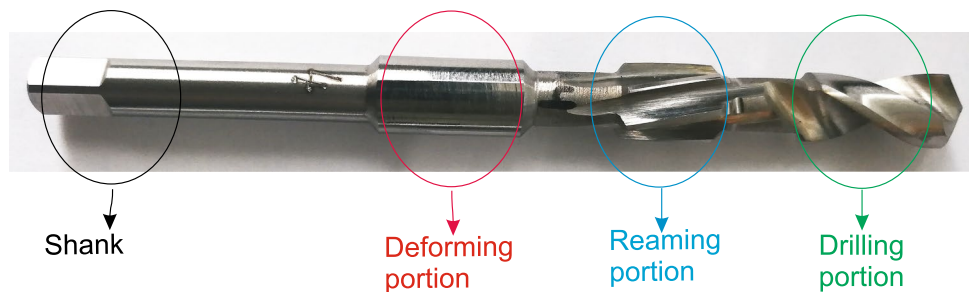
Based on the conducted experimental studies and the results obtained, in order to increase the productivity of machining by plastic deformation of small fastener holes

in high-strength aluminum alloys, a super-combined tool with four walls of the deforming portion was developed combining successive drilling, reaming and plastic deformation of the hole (Fig. 17). The diameter D of the circumscribed circle over the tool deforming portion is 8.25 mm. The diameters of the drill and reamer sections are selected so that the nominal interference fit for the third section is $i = 0.07$ mm. With the obtained optimal values of the governing factors for plastic deformation ($v = 22.5$ m/min and $f = 0.025$ mm/rev) series of 50 holes in samples made of 2024-T3 Al alloy are machined on Haas MiniMill machining center. Very good repeatability of the surface area of the holes is observed, whereby the resulting roughness fluctuates around $R_a = 0.552$ μ m.

7 Conclusions

- Novel method and tool for cold plastic deformation of a large number of fastener holes in high-strength Al alloy structures have been developed aiming to decrease labor and operational time by complying with the requirement of high fatigue resistance. This method can be carried out on both conventional and CNC machines, as well as on manually operated machines.
- Through an experiment and FEM simulations, the most optimal values of the governing parameters of the cold plastic deformation process have been found using the proposed method and tool.
- The method and tool produce three main beneficial effects: HCE, SPD and MSM. The first of them is expressed in the introduction of beneficial residual hoop compressive stresses around the hole at a significant depth. The benefit of SPD is expressed in the following: (1) burnishing of the surface layer with a significant reduction of the initial roughness—from $R_a \approx 1.4$ μ m to

Fig. 17 New combined tool



$R_a \approx 0.5 \mu\text{m}$; (2) coldwork of the surface layer with a substantial equivalent deformation and, respectively, a notably increased microhardness; (3) residual compressive stresses in the surface and subsurface layers. MSM of the hole surface and subsurface layers is observed. The microscopic analysis shows significant grain refining. Due to specific method's kinematics and deforming tool geometry, local torsion of the surface and subsurface layers is observed. As a result of the HCE, SPD and MSM effects, the fatigue life of flat specimens with fastener holes that have been processed using the proposed method and tool, is increased significantly in comparison with specimens whose holes have only been drilled and reamed.

- A super-combined tool that consequently performs drilling, reaming and cold plastic deformation is designed and manufactured. This tool significantly increases the productivity of processing a large number of fastener holes in aluminum structures. To make a comparison, the split sleeve method is carried out in 5 main steps which do not include the steps of control, while the super-combined tool can perform the proposed method in single step.

Acknowledgements This work was supported by the Bulgarian Ministry of Education and Science and the Technical University of Gabrovo under Contract No. 1801M. The authors extend their special acknowledgements to Dr Yosiph Mitev and Dr Dobri Petkov for his collaboration with the experiments.

References

1. Champoux LA (1971) Coldworking method and apparatus. USA Patent 3566662, 2 Mar 1971
2. Duncheva GV, Maximov JT, Ganey N (2017) A new conception for enhancement of fatigue life of large number of fastener holes in aircraft structures. *Fatigue Fract Eng Mater Struct* 40(2):176–189
3. Mishra RS, Mahoney MW, McFadden SX, Mara NA, Mukherjee AK (2000) High strain rate superplasticity in a friction stir processed 7075 Al alloy. *Scripta Mater* 42:163–168
4. Mishra RS, Ma ZY, Charit I (2003) Friction stir processing: a novel technique for fabrication of surface composite. *Mater Sci Eng A* 341:307–310
5. Hogenhout F (1987) Method and apparatus for hole coldworking. USA Patent 4665732, 19 May 1987
6. Maksimov YT, Duncheva GV (2014) Device and tool for cold expansion of fastener holes. USA Patent 8915114, 23 December 2014
7. Maximov JT, Duncheva GV, Amudjev IM (2013) A novel method and tool which enhance the fatigue life of structural components with fastener holes. *Eng Fail Anal* 31:132–143
8. Easterbrook ET (2001) Method and apparatus for producing beneficial stresses around apertures by use of focused stress waves, and improved fatigue life products made by the method. USA Patent 6230537, 15 May 2001
9. Easterbrook ET, Flinn BD, Meyer CA, Juhlin N (2001) The Stress-Wave™ Fatigue Life Enhancement Process. In: Proceedings of the 2001 aerospace congress, Seattle, Washington, 10–14 Sept 2001
10. Korzynski M (2013) Slide diamond burnishing. In: Korzynski M (ed) *Nonconventional finishing technologies*. Polish Scientific Publishers PWN, Warsaw, pp 9–33
11. Nee AYC, Venkatesh VC (1982) Bore finishing—the ballizing process. *J Mech Work Technol* 6(2–3):215–226
12. Maximov JT (2002) Spherical mandrelling Method implementation on conventional machine tools. *Int J Mach Tools Manuf* 42(12):1315–1325
13. Catalogue Ecoroll (2006) Tools and solutions for metal surface improvement. Ecoroll Corporation Tool Technology, Milford
14. Christ RJ, Nardiello JA, Papazian JM, Madsen JS (2010) Device and method for sequentially cold working and reaming a hole. USA Patent 7770276, 10 Aug. 2010
15. Korzynski M (2009) A model of smoothing slide ball-burnishing and an analysis of the parameter interaction. *J Mater Process Technol* 209(1):625–633
16. Korzynski M (2007) Modeling and experimental validation of the force-surface roughness relation for smoothing burnishing with a spherical tool. *Int J Mach Tools Manuf* 47(12):1956–1964
17. Maximov JT, Duncheva GV, Anchev AP, Ganey N, Amudjev IM, Dunchev VP (2018) Effect of slide burnishing method on the surface integrity of AISI 316Ti chromium–nickel steel. *J Braz Soc Mech Sci Eng* 40:194. <https://doi.org/10.1007/s40430-018-1135-3>
18. Maximov JT, Anchev AP, Duncheva GV, Ganey N, Selimov KF (2017) Influence of the process parameters on the surface roughness, micro-hardness, and residual stresses in slide burnishing of high-strength aluminum alloys. *J Braz Soc Mech Sci Eng* 39(8):3067–3078
19. Shamdani AH, Khoddam S (2012) A comparative numerical analysis of combined cold expansion and local torsion on fastener holes. *Fatigue Fract Eng Mater Struct* 35(10):918–928

Publisher's Note Springer Nature remains neutral with regard to jurisdictional claims in published maps and institutional affiliations.